

## The influence of process parameters in friction stir welding of Al-Mg alloy and polycarbonate

Hamed Aghajani Derazkola<sup>a,\*</sup>, Majid Elyasi<sup>b,\*</sup>

<sup>a</sup> Young Researchers and Elites Club, Science and Research Branch, Islamic Azad University, Tehran, Iran

<sup>b</sup> Faculty of Mechanical Engineering, Babol Noshiravani University of Technology, P.O. Box 484, Babol, Iran



### ARTICLE INFO

#### Keywords:

Friction stir welding  
Polycarbonate  
AA5058 aluminum alloy  
Material flow  
Dissimilar joint  
Mechanical property

### ABSTRACT

The Role of rotating and travelling speed of the friction stir welding (FSW) tool on the dissimilar lap-joining of an AA5058 aluminum alloy and polycarbonate (PC) sheets has been investigated. The Relation of the processing parameters with tensile, bending strength, material flow and hardness of the joints were studied to attain defect-free joints with proper mechanical strength. The results showed both the size and the contribution of PC and aluminum alloy on the formation of stir zone are strongly related to the tool's rotational speed. Tool's rotational speed mainly controls the joint strength and the fracture mode, while traverse velocity affects the size of aluminum fragments within the PC matrix. The most suitable dissimilar lap-joining microstructure is achieved at 1600 rpm and 45 mm/min tool speed. Under this condition, the maximum joint tensile and bending strengths attained are 68.2% (46 MPa) and 69.4% (60 MPa) of PC raw material respectively. Fractography indicated that during the tensile test, the rupture occurs below and in the middle of the stir zone on AA5058 alloy/PC interface during the bending test. The hardness of the PC after FSW decreased by the molecular weight reduction and AA5058 micro-hardness increased because of the fine grinding after suffering thermo-mechanical cycle.

### 1. Introduction

Recently, especially in automotive industries, widely used metals like steel are being replaced by the new lighter nonferrous materials such as magnesium and aluminum alloys [1]. In addition, polymer technology developments led into modern structures [2–4]. Modern thermoplastic materials as a specific type of polymer for having reshaped properties, are used in different engineering applications, such as automotive and aerospace industries, due to their lower cost, high toughness and stress ratios compared to their weight [3]. These are one of the most commonly used materials in many industrial applications due to their easy manufacturing process [5]. Even though thermoplastic materials offer wider choice of design or process, manufacturing of bigger and complex parts frequently need joining to different materials and alloys [6,7]. These materials can be integrated with the polymer-metal hybrid technologies in a monadic component [8–10]. Studies and developments of such hybrid structures which led to the reduction of the weight of structures is increased in recent years. Lower fuel usage and CO<sub>2</sub> emission are the main factors that persuade the engineers to produce these lightweight structures [11,12]. Joining of polymer-metal hybrid structures is more difficult by traditional welding process due to their big difference in physical and chemical features [13]. Metal-

polymer joining limitations such as surface treatments and adhesive bonding time, motivated novel joining techniques [14].

Amancio et al. classified various polymer-metal hybrid structures joining technologies from more conventional process like adhesive bonding to novel welding-based technologies like ultrasonic and inductive welding process [7,15,16]. Abibe et al. used a technology, based on staking and mechanical fastening which is called “injection clinching joining” to investigate the mechanical and failure behavior of the polymer-metal joints [17]. Lambiase and Paoletti joined thin aluminum sheets with Carbon Fiber Reinforced Polymer (CFRP) laminates by friction assisted clinching and showed that in this process the material formability increased and defect free joint was achievable even with sharp tool [18,19]. Blaga et al. investigated joining of the titanium grade 2 with the glass-fiber-reinforced thermoplastic composites by friction riveting technique [20]. Feasibility study, mechanical properties and optimization of ultrasonic spot welding of aluminum and carbon-fiber reinforced polymers (CFRP) is carried out by Balle et al. [21,22]. They also studied the process parameters to achieve the quasi-static tensile shear strength of up to two times higher than the weakest base alloy. Goushegir et al. investigated the weldability of AA2024 and CFRP using different post heat treatments, which resulted in joints with significant shear strength [23,24]. The feasibility of induction welding

\* Corresponding authors.

E-mail addresses: [h.aghajany@gmail.com](mailto:h.aghajany@gmail.com), [hamed.aghajani@srbiau.ac.ir](mailto:hamed.aghajani@srbiau.ac.ir) (H.A. Derazkola), [elyasi@nit.ac.ir](mailto:elyasi@nit.ac.ir) (M. Elyasi).

of steel and Al-Mg alloy with CFRP was investigated and by Mitschang et al. [25]. They also studied the effect of different metal surface pre-treatments on the joint shear strength. However, due to the high manufacturing cost and equipment complexity of aforementioned welding methods, developing a new welding process is still needed [1]. Constant efforts are going on to develop and improve alternative joining techniques for these hybrid structures, such as the infrared welding, friction stir welding and the forced mixed extrusion technique [26]. One important advantage of the mentioned processes compared with the regularly used mechanical fastening or adhesive techniques is the higher assembly rates and consequently lower assembly costs. FSW is a rapidly developing solid state joining process with reduced material waste and without radiation or harmful gas emissions which are usually associated with the fusion welding techniques [27]. In FSW process, a hard rotating tool and a pin is inserted in the butting edges of the sheets traverse along the joint line [28]. Due to the friction and deformation between tools and surrounding materials, heat will be generated [29]. The tool rotation and traverse expedite material flow from the front to the back of the pin and welded joint are produced [30].

Accordingly, there are a number of researches on the possibility of using friction base process to join metals to polymers. Amancio-Filho et al. investigated on the feasibility of friction spot joining between AZ31 magnesium and CFRP composites and showed that metallurgical and physicochemical transformations of polymer take place during welding [4]. Yusof et al. studied on friction spot welding of AA5052 aluminum and PET and concluded that a successful joint produced with the aid of frictional heat energy generated from the FSSW process [30]. They showed that the plunge speed had a significant influence on the heat affected area while joined area was relatively reducing as the plunge speed increased. Goushegir et al. studied on the friction spot welding of AA2024 aluminum alloy and carbon-fiber reinforced poly(phenylene sulfide) composite [23]. They revealed that higher rotational speed of the tool lead to the highest shear strength of the formed joint. Lambiase et al. joined PVC and AA5053 aluminum alloy with friction assist joining [31–33]. They revealed that by controlling the plunge force, dwell time and clamping frame material, it is possible to achieve a joint with 97 percent of PVC strength. Lambiase and Paoletti also studied on friction assist joining of AA5053 aluminum alloy and poly etherether ketone (PEEK) [32]. They showed that with laser texturing of aluminum surface, achieving a joint with about 83% PEEK strength is possible. Khodabakhshi et al. studied the bonding mechanism, joint strength, and micro-hardness of friction stir welding of AA5059 aluminum alloy and high density polyethylene (HDPE) [34]. A maximum joint strength ratio improvement up to 50% with failure location from the interface of stir zone with aluminum alloy was reported. They examined the main bonding mechanisms and the nature of interface during dissimilar friction stir joining of aluminum and polymer with employing the scanning- (STEM) and high resolution-transmission electron microscopy (HR-TEM) [34]. As a result, mechanical interlocking and secondary Vander Waals interaction assisted by chemical bonding with formation of a thin alumina layer at the interface have been introduced as the main mechanisms. Liu et al. used friction lap welding for joining AZ31B Mg alloy and MC Polyamide 6 (Nylon 6). They showed that increasing welding speed, tool rotation rate and plunge depth will help to reduce the volume of bubbles in joint line and produce the strongest joint with area fraction of 8% bubbles [35]. Ratanathavorn et al. welded AA6111 aluminum alloy to polyphenylene sulphide (PPS) by FSW process. They indicated that the welding stir zone contained a blend of AA6111 aluminum alloy particles and chips which restricted by PPS matrix [36]. The sizes and shapes of the AA6111 alloy fragments in the stir zone are closely related to the travelling speed as rapid linear speeds tend to create coarser fragments. Shahmiri et al. studied on FSW of aluminum alloy to polypropylene sheets [37]. They indicated that shear strength of the joints decreased by the growth of the heat-input due to the increase in the thickness of the interaction layer. The maximum shear-tensile strength of this joint

was about 20% of the shear strength of polypropylene. In the present study, the effects of tool's rotating and travelling speed of the overlap joint with AA5058 aluminum-magnesium alloy to transparent polycarbonate (PC) was investigated by using FSW. The tool used in this work generated aluminum fragments instead of plasticizing. Simultaneously, the PC melted and merged into the chipped zone to form a joint. Formation of joint mechanisms were studied in terms of the materials flow pattern as characterized using optical microscopy (OM) and scanning electron microscopy (SEM) equipped with energy dispersive X-ray spectroscopy (EDS) analysis. The prepared dissimilar FSW joints were evaluated in terms of joint strength, fracture behavior, hardness and microscopic examination of the weld cross-section to find out the optimum working window with maximum improvements in the mechanical performance.

## 2. Experimental procedure

An AA5058 aluminum-magnesium alloys and polycarbonate (PC) polymer sheets utilized as the raw base materials. These plates were cut in the dimensions of  $200 \times 50 \times 3$  mm by using water-jet machine. AA5058 alloy is commonly used for automobile sheet panels and PC is a special thermoplastic which shows good thermal and chemical stability that is usually being used for lighting systems and external parts of automobile body. These initial materials have potential application in automobile body structure. The physical properties of the selected initial materials are presented in Table 1.

The lap-joint design with placing the PC on top was examined during the friction stir welding for processing an AL-polymer bi-material structure from these dissimilar initial materials. A flexible clamping system made of carbon steel with two supporting plates was designed to clamp the raw sheets during the welding process in their proper positions. Single-pass friction stir welds were conducted using a milling machine, in position control, and FSW tool was made of tungsten carbide. The schematic view of plates and clamping system, tool plunge depth and tilt angle is shown in Fig. 1a and b, respectively.

Real thermal histories during FSW process were monitored by placing a 0.5 mm diameter K-type thermocouple (Omega Engineering, USA) inside the different regions of aluminum-side and 0.5 mm diameter J-type thermocouple (Omega Engineering, USA) in PC-side. The J-type thermocouple was attached into PC holes with Testor's cement for plastic material and held for 12 h before welding process to allow the glue to set. Thermocouples with 0.5 mm diameter were embedded into the interface of sheets at a distance of 5, 10, 15 and 20 mm from the joint center at aluminum side and 5, 10 and 15 mm from joint center in PC side. The schematic view of thermocouple places has been shown in Fig. 1c.

The maximum temperature obtained during the process was recorded at each rotational speed. A wide range of FSW tool speeds including the various tool rotating and travelling speed with constant tool tilt angle and tool plunge depth were assessed to establish a suitable working window for producing a defect-free dissimilar joint with

**Table 1**

The main physical properties of AA5058 aluminum alloy and polycarbonate (PC) polymer.

Base materials	AA5058	PC
Density ( $\text{kg/m}^3$ )	2685	1220
Ultimate tensile strength (MPa)	145	66.3
Elongation (%)	24	98
Bending strength (MPa)	240	88
Shear strength (MPa)	103	101
Microhardness (HV)	50	–
Hardness (Shore D)	–	90
Glass transition temperature ( $T_g$ )	–	147 °C
Melting point (°C)	591	225
Thermal conductivity at 25 °C (W/m.K)	193	0.22

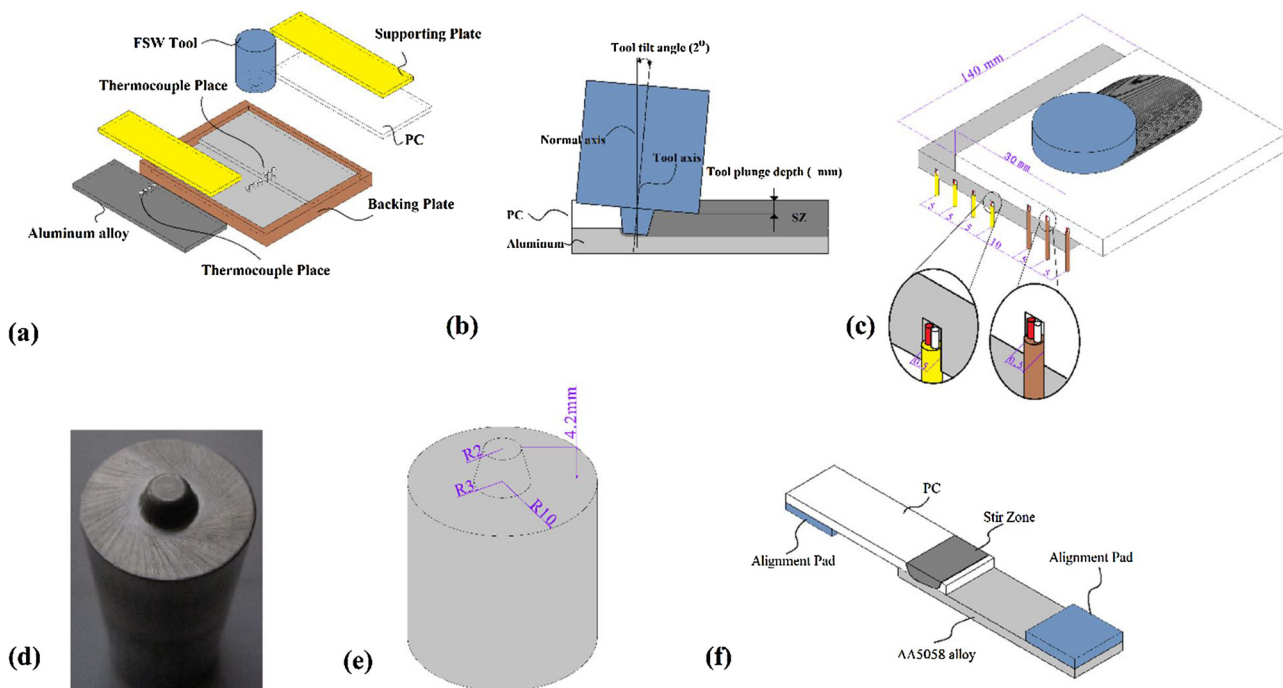


**Fig. 1.** (a) schematic view of clamping system, (b) process variable, (c) K- thermocouples places, (d) FSW tool, (e) FSW tool dimension, (d) FSW sample which is used in tensile and bending test.

**Table 2**

The process parameters in FSW of AA5058 aluminum alloy and polycarbonate (PC) polymer.

Parameter	Value
Tool rotational speed (rpm)	960, 1200, 1600 and 1940
Tool travelling speed (mm/min)	45 and 90
Tool tilt angle (degree)	2
Tool plunge depth (mm)	0.3

acceptable surface appearance. **Table 2** summarizes the experimental plan.

A 20 mm diameter tool shoulder with a conical probe measuring 4 to 6 mm in diameter (smallest and biggest ones) with 4.2 mm in length was used in this work which is shown and modeled in Fig. 1d and e, respectively. For accomplishment in macro- and micro-structural investigations, the metallographic samples were prepared parallel and perpendicular to the FSW direction from the dissimilar joints to examine the bonding mechanism and formation at two different cross sections.

The standard metallographic procedure including grinding with using different grades of emery SIC papers and final mechanical polishing of diamond pastes was performed on the samples. Materials flow patterns in the stir zone (SZ) of two dissimilar initial materials and their inter-mixing were studied under an optical microscope (OM) incorporated with an image analyzing software (Clemex-Vision). Also, a scanning electron microscope (SEM, VEGA//TESCAN-XMU, RUSSIA) equipped with energy-dispersive X-ray spectroscopy (EDS) was utilized to analyze the interaction between aluminum and polymer during FSW process for finding the contributed bonding mechanisms and increasing the quality of SEM images. Tensile and bending test was carried out for evaluation of the mechanical behavior of the joints. During the tests, an alignment pad is set on AA5058 alloy and PC sheet to align the initial materials into the testing machines. A schematic of the specimen is depicted in Fig. 1f. For each welding condition, tensile and bending test was repeated three times and average values have been reported. Shore hardness test was applied to study the change in hardness of the PC

side. Micro-hardness test was carried out to study on the hardness changing of AA5058 alloy side.

### 3. Results and discussion

#### 3.1. Thermal history

Fig. 2a shows a sample of recorded thermal history of the joints welded with 1600 rpm rotational and 45 mm/min tool travelling speed. According to the measured temperature of the joint area, the temperature rises sharply to the peak temperature and then remains constant for a short time and after that cooling stage begins. Materials were pre-heated at the leading side during the progresses of the FSW tool and after stirring action cooled down at the trailing side of the tool [2]. Due to the low thermal properties of the PC, the pre-heating and initial deformation areas in front of the tool are shrunk to a thin layer, and the final cooling stage of the joint line is very slow. This material properties caused the temperature fields to remain high at the joint line even after moving forward of the FSW tool. This trend repeated for all samples of all tool speeds. The results of the previous research on FSW of polymers showed that the cooling rate of the stir zone was very slow and the temperature drop rate remained almost constant near the maximum temperature for a long time after moving FSW tool from stir zone [38]. Due to the location of the PC at the top of the aluminum alloy in this study, it seems that after moving the FSW tool (heat source) from welding area, higher heat transfer coefficient of aluminum alloy will increase the cooling rate of stir zone. After a short time, the frictional heat in stir zone starts to diffuse in other area of the initial materials and temperature of the stir zone begins to decrease.

In this condition, direct contact of aluminum alloy with stir zone helps to speed up the cooling rate. The delay caused by starting to rapid cooling rate in stir zone is the period by which FSW AA5058 alloy needs to lose its temperature and frictional heat diffuse from joint area into AA5058 aluminum alloy and PC sheet. The results of the delay time cooling rate for each welding condition have been shown in Fig. 2b. As can be seen, by increasing the heat input, the delay time increases. For instance the delay time for a joint welded with 960 rpm and 90 mm/m

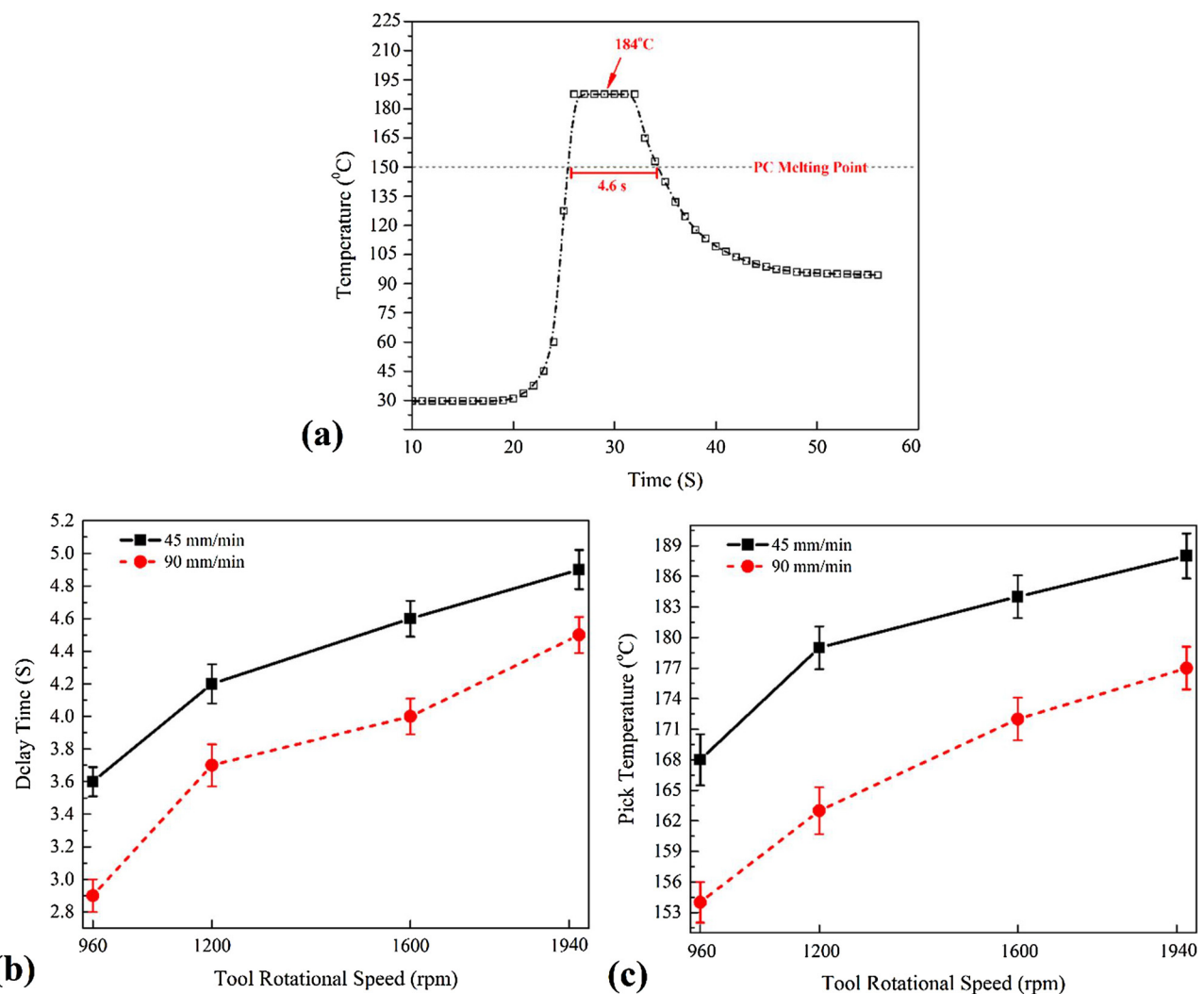


**Fig. 2.** (a) thermal history of the joint welded with 1600 rpm tool rotational and 45 mm/min tool travelling speed, (b) starting cooling time delay, (c) recorded peak temperature at various tool speed.

min was 2.9 s and corresponding delay time with 1940 rpm and 45 mm/min tool speed was 4.9 s. The results of the recorded temperature showed that generated heat in all welding parameters were higher than the melting point of PC raw material. It seems that this phenomenon is the result of high stirring action of FSW tool and generated heat at aluminum side which led to the production of the frictional heat in stir zone. Due to the selected parameters in this study, the maximum temperature produced with 1940 rpm and 45 mm/min tool speed is ~189 °C and the minimum temperature produced in 960 rpm and 90 mm/min tool speed is ~154 °C. The recorded peak temperature in this study has been shown in Fig. 2c.

### 3.2. Surface material flow

The surface flow of the base material in dissimilar FSW joint indicates the surface mixing by tool shoulder [39]. Due to the huge difference in physical and chemical properties of polymers and metals, study on the surface flow of the PC and aluminum alloy helps to better understanding of the mixing quality of base materials. Fig. 3a and b shows the top view of joint line which welded with 1940 rpm (45 mm/min) and 960 rpm (90 mm/min) tool speed respectively. It should be noted that formed joint lines are grey, while the used PC sheet is colorless. It seems that the mixing of aluminum alloy and PC sheet has led to the formation of the grey joint line. The high magnified SEM image

from the surface of the joint which welded with 1940 rpm (45 mm/min) is shown in Fig. 3c. The obtained results indicate that the small AA5058 alloy particles are spread over the PC matrix after FSW process. Subsequently, the combination of aluminum fragments and polycarbonate cause the joint line to appear grey. In Fig. 3c, the aluminum particles are white. EDS spectra from of the corresponding particle is shown in Fig. 3d.

According to the process setup in this study, the PC sheet located at the top and AA5058 sheet was at the bottom. This arrangement led to the direct contact of the tool shoulder with PC and also the tool pin with AA5058 aluminum alloy. It seems that despite the differences in density of the aluminum particles and plasticized PC, tool axial and forging force caused the suspended AA5058 fragments from lower area of SZ extruded into the upper area and after cooling phase, this particles remain in all regions of it. The results show that the heat affected zone (HAZ) was formed in the vicinity of joint line that were the results of heat diffusion beside the SZ area which is produced by tool shoulder in all samples. The formation of HAZ area in friction stir processing of the polymeric materials is the result of orientation changes of the polymer chains taking place beside the joint line. As a result, the refraction index of the welded area changes [40]. Due to the FSW tool rotation direction, the stirring action and heat concentration are more in advancing side (AS) than the retreating side (RS). This material behavior during FSW process caused the heat diffusion to be more in AS that has led to the

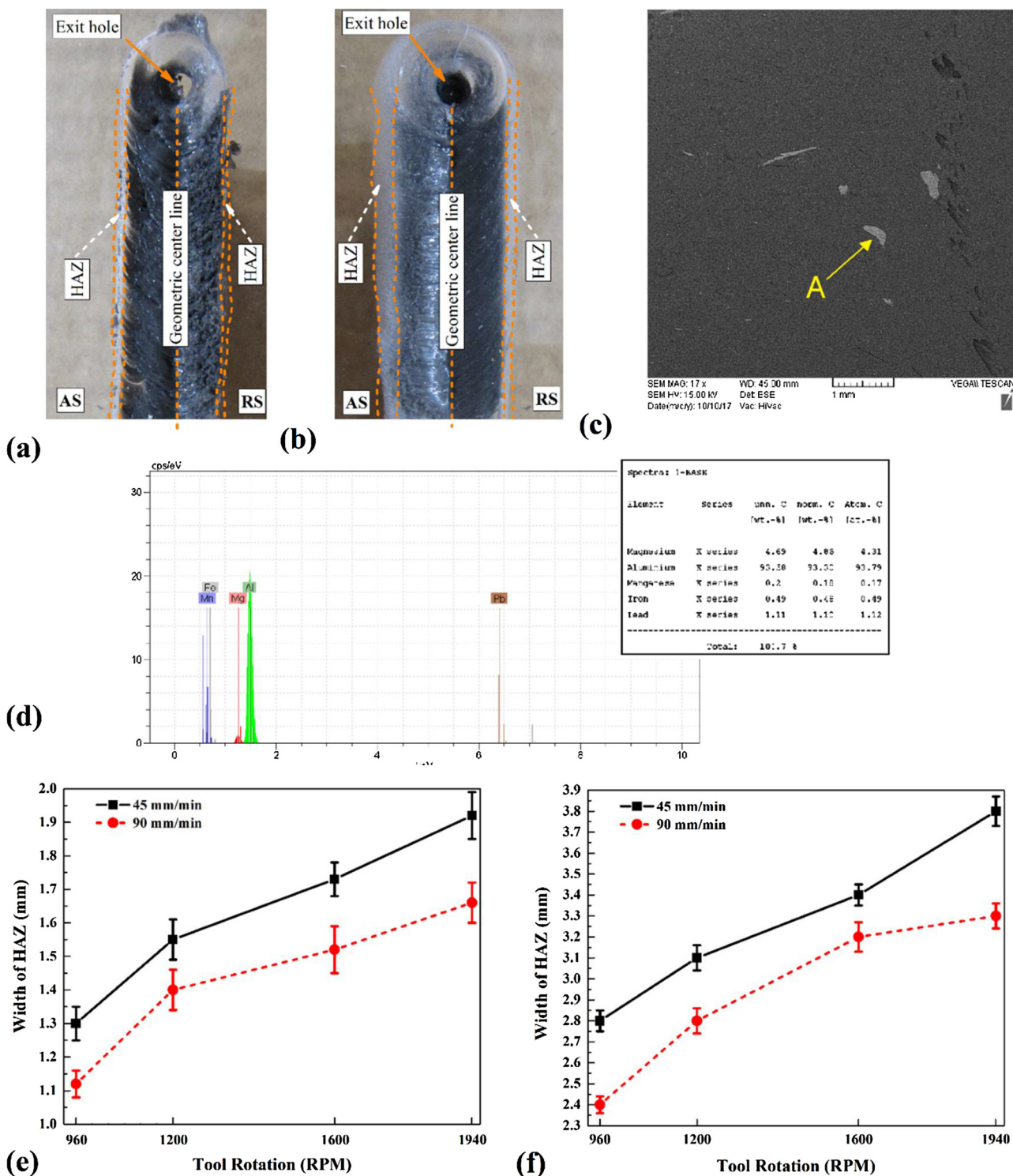


**Fig. 3.** Surface material flow of joint with 1940 rpm tool rotation and 45 mm/min tool travelling speed, (b) 960 rpm tool rotation and 90 mm/min tool travelling speed, (c) SEM image from aluminum particle in top surface of joint line, (d) EDS spectra from aluminum particle in top surface joint line, (e) width of HAZ in AS, (f) width of HAZ in RS.

formation of bigger HAS in AS. The HAZ area width in AS and RS of joint's top surface is presented in Fig. 3e and f, respectively. As can be seen, by increasing the heat input (high tool rotation and/or low tool travelling speed) the HAS area width in both AS and RS has been increased. According to the results, the widest HAZ area is formed in the top surface (AS and RS) of joint with welding condition of 1940 rpm (45 mm/min) tool speed and the thinnest HAZ area is formed in top surface (AS and RS) of joint which welded with 960 rpm (90 mm/min)

tool speed.

### 3.3. Macrostructure of joint

The cross section view of joints that has been shown in Fig. 4 indicates that the stir zone (SZ) is formed as polymer-metal composite by mixing the PC matrix and aluminum particles reinforcement. According to the results, a narrow heat affected zone (HAZ) was formed on the

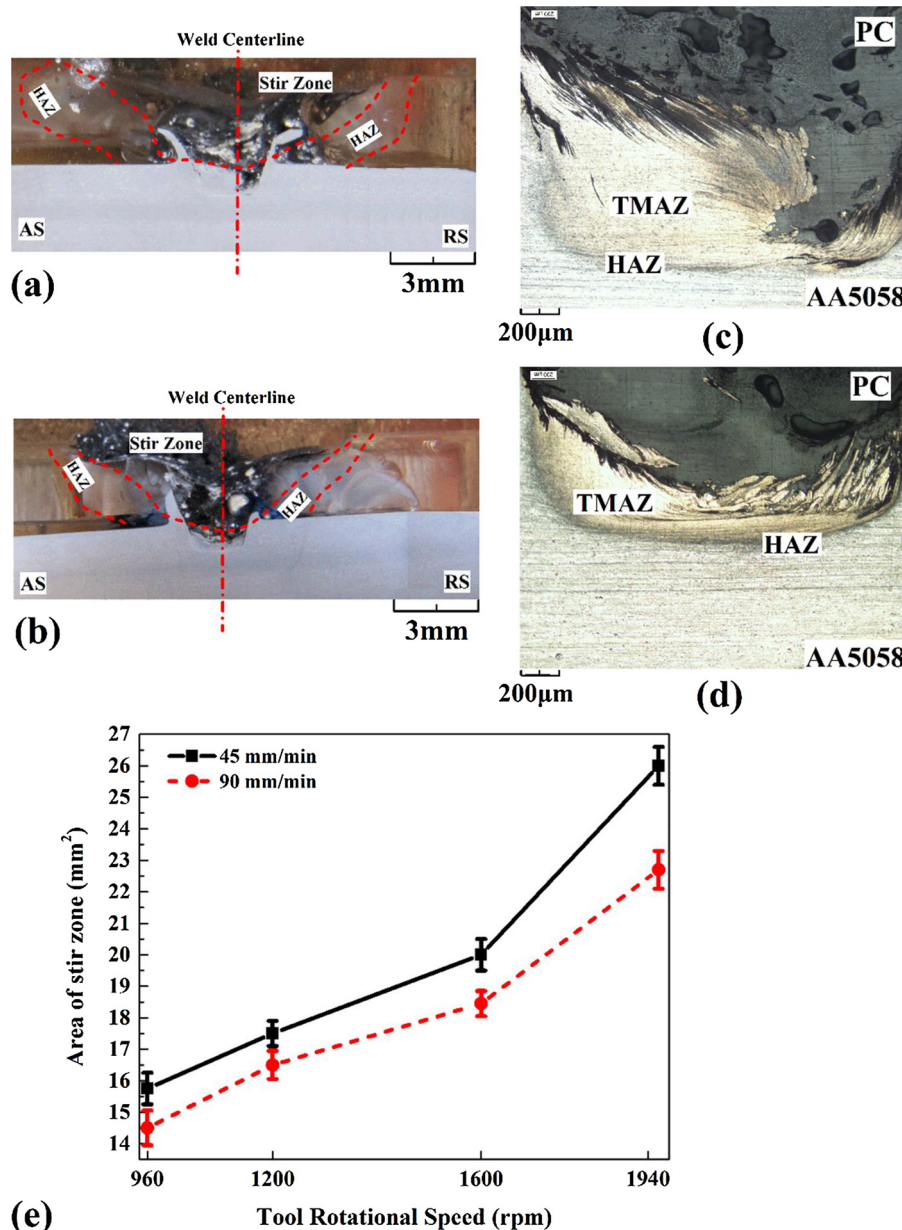


**Fig. 4.** cross section view of joints which welded at (a) 1600 rpm tool rotation and 45 mm/min travelling speed, (b) 960 rpm tool rotation and 90 mm/min travelling speed, (c) microstructure of TMAZ and HAZ area in joint that welded at 1600 rpm tool rotation and 45 mm/min travelling speed, (d) microstructure of TMAZ and HAZ area in joint that welded at 960 rpm tool rotation and 90 mm/min travelling speed, (e) area of SZ at different tool speed.

sidelines of SZ in PC side. As previously discussed, HAZ in PC is unsoften narrow area which is formed by diffusion of the heat from SZ (soften PC) [35]. Interface of HAZ and SZ is the result of reduction in the inter-diffusion of molecules over the interface. The interface in this area was probably maintained by the secondary forces (e.g., Vander Waals) associated with the wetting phenomenon between SZ and HAZ giving rise to a weld line [40]. A thermo-mechanical (TMAZ) and narrow heat affected zone (HAZ) were formed in AA5058 aluminum alloy side. The results showed that the HAZ area in advancing side is larger than the retreating side. This phenomenon is common in FSW process due to the rotation direction of the tool. The cross section view of joints which welded at 1600 rpm (45 mm/min) and 960 rpm (90 mm/min) has been shown in Fig. 4a and b, respectively. It seems that during FSW process, tilted pin, penetration aluminum base metal led to the high mechanical work rate. Subsequently, the AA5058 twisted around the pin and the produced tow ramus in advancing and retreating side along the joint line. Due to the rotation direction of tool,

the concentration of frictional heat and thermomechanical work (strain rate) in advancing side is more than the retreating side [25], therefore the formed ramus in advancing side is also larger than the retreating side. Because the tool shoulder and AA5058 alloy didn't have any contact, the generated heat by shoulder in the surface of PC was not enough till plasticized aluminum. Moreover, the low heat transfer properties of PC led to the low amount of heat transfer to an aluminum alloy. This phenomenon caused the aluminum surface to place under the mechanical deformation cycle just by the FSW tool pin. As can be seen, the TMAZ was formed in the lower area of SZ in AA5058 alloy side which is brown in OM picture. In the OM image, the TMAZ is surrounded by a dark thin heat affected zone (HAZ) in aluminum side.

The high magnification of the OM image of the joints area which welded at 1600 rpm (45 mm/min) and 960 rpm (90 mm/min) is shown in Fig. 4c and d, respectively. The results shows that by decreasing the tool rotating speed and increasing its travelling speed, the formed joint area becomes smaller. The measuring area of SZ at different tool speeds

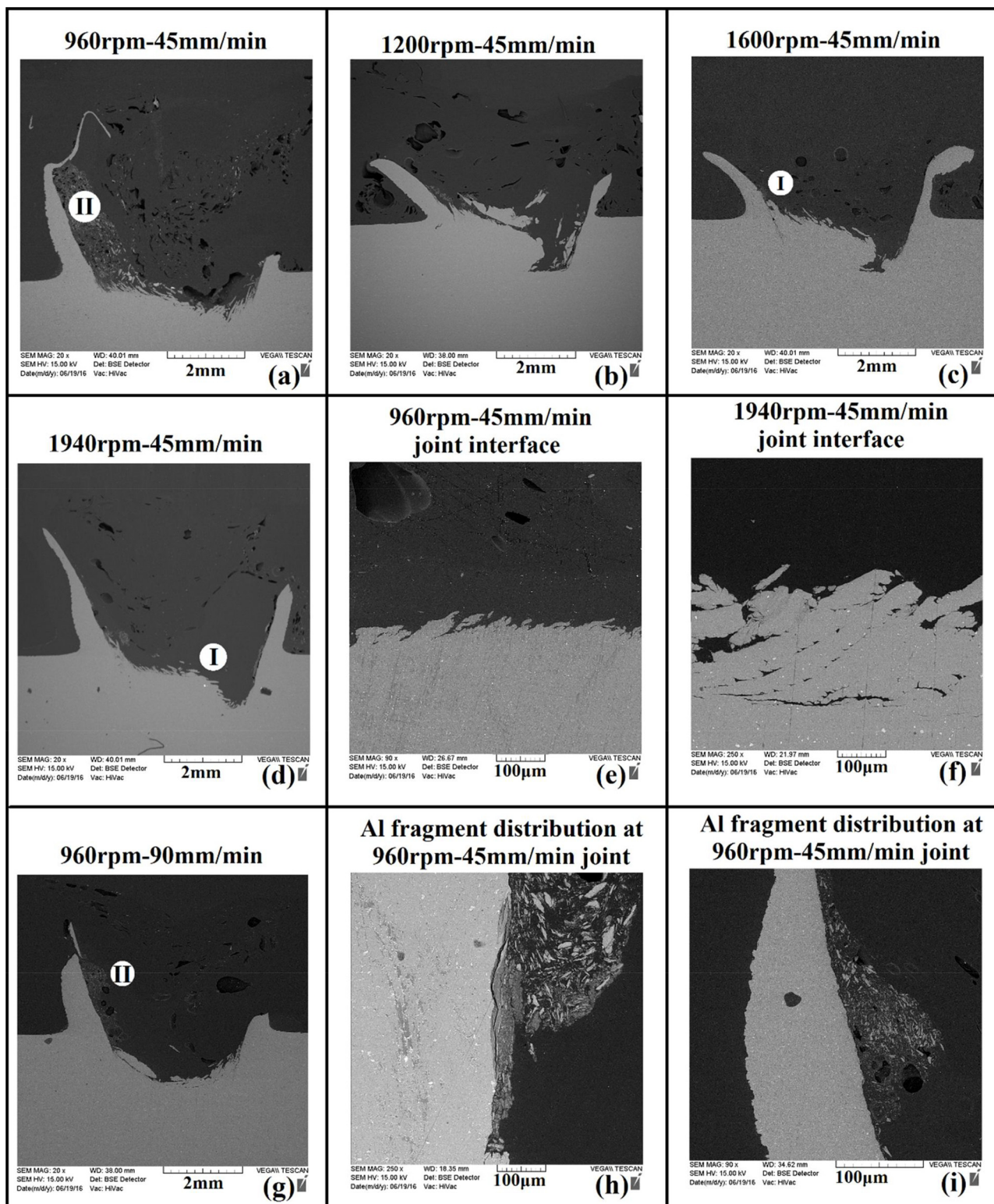


**Fig. 5.** Cross section SEM image from joints which welded at 45 mm/min tool travelling and (a) 960 rpm, (b) 1200 rpm, (c) 1600 rpm and (d) 1940 rpm tool rotational speed. Thickness of mechanical interlock that produce in (e) 1600 rpm (45 mm/min) and (f) 1940 rpm (45 mm/min) tool speed. (g) internal flow of joint which FSW at 960 rpm (90 mm/min) tool speed. Distribution of AA5058 fragments on AS of joints that FSW at (h) 45 mm/min (960 rpm) and (h) 90 mm/min (960 rpm) tool speed.

shows that the bigger stir zone is formed with increasing tool rotational speed and decreasing tool transverse speed. According to the 2D measurement of SZ that depicted in Fig. 4e, the biggest area formed at 1940 rpm and 45 mm/min tool is  $\sim 26 \text{ mm}^2$  and the smallest area formed at 960 rpm and 90 mm/min tool is  $\sim 14.5 \text{ mm}^2$ . The SEM image

from cross section view of joints welded at 45 mm/min traverse speed and 960, 1200, 1600 and 1940 rpm tool rotational speed has been shown in Fig. 5a–d, respectively. As can be seen, the thermomechanical cycle in aluminum side helped the formation of wavy dents in the interface of AA5058 TMAZ and SZ by tool pin in all joints. The aluminum

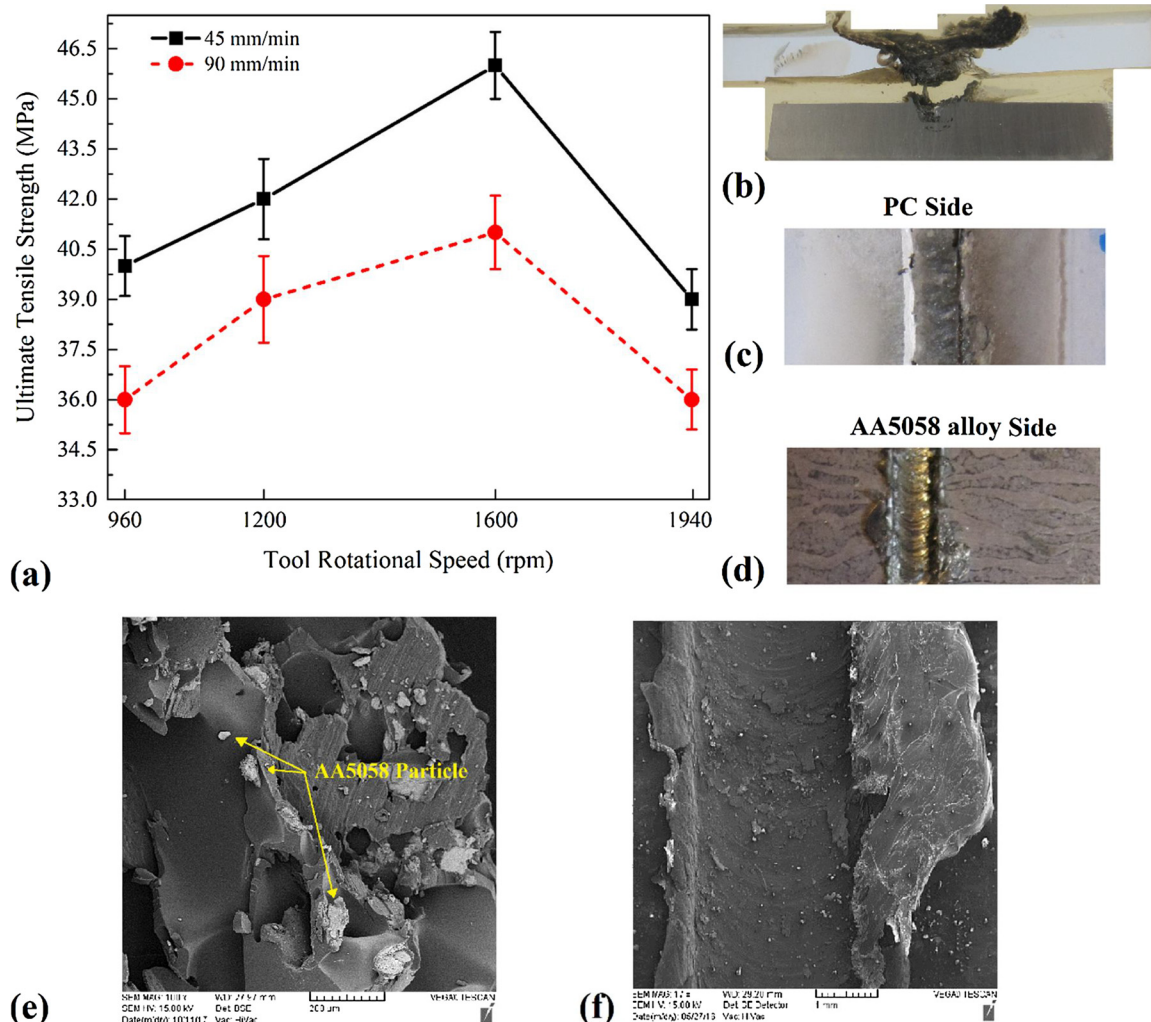


**Fig. 6.** (a) Tensile strength of the joints. (b). Electronic image from tensile test (c).fracture surface of PC9 side (d).AA5058 side. (e).SEM image from fracture surface of PC side (f) AA5058 side.

wavy dents increased mechanical interlock between AA5058 and PC in the lower area of SZ. The results showed that by increasing tool rotational speed the length and width of aluminum ramus in advancing and retreating side will increase. The increasing tool rotational speed caused to the growth of the thickness of mechanical interlocks in SZ. The marked area (point of I) from lower area of SZ in joint which FSW at 1600 rpm and 1940 rpm rotational speed is shown in Fig. 5e and f, respectively. The growth of the thickness of mechanical interlocks by increasing tool rotational speed is evident in this area. Some tiny aluminum particles were spread in PC matrix that fractured from AA5058 alloy during stirring action. With increasing heat input, the wavy dents become thicker and AA5058 alloy fragments become larger. The SEM image from cross section view of joint welded at 960 rpm and 90 mm/min tool speed is shown in Fig. 5g. As can be seen, by decreasing the heat input with tool travelling speed, thermomechanical action of the tool in SZ decreases and the presence of AA5058 fragments decreases in PC matrix. The marked area (point of II) from joint which FSW at 45 mm/min (960 rpm) and 90 mm/min (960 rpm) tool speed is shown the phenomenon which depicted in Fig. 5h and i, respectively. The results also revealed that adjacent AA5058 alloy particles and some voids were formed in SZ which can decrease the mechanical properties of the joints. The thermal study showed that the peak temperature in FSW of PC/AA5058 alloy was more than the melting point of the polycarbonate sheets in most of the samples which caused the PC sheet to melt and re-solidify after FSW process. This phenomenon caused

some chemical changes in the structure of the PC sheet. Shrinkage properties and moisture absorption are two key factors that caused the bubble formation in SZ [41–43]. During the FSW, the melted PC absorbs the air moisture that is in hot environment (melted PC) and turns it to vapour and consequently vapour expansion creates tiny bubbles in SZ. At high tool travelling and rotational speeds, the PC doesn't have enough time to drag more air during the joining phase which caused the vapour expansion bubble to decrease in high tool travelling and rotational speed. On the other hand, the melted PC, due to its physical properties starts shrinking after cooling stage in SZ which caused the formation of some shrinkage bubbles (internal cavities) and a gap between aluminum alloy and PC in SZ. Melting and re-solidification of thermoplastics cause them to lose their molecular weight and this phenomenon exacerbates their shrinkage properties which may decrease the mechanical strength of joint and consequently formation of weak SZ [44]. According to the results, by controlling the heat input in SZ, the size and numbers of shrinkage bubbles can be minimized. The optimum joint window with admissible voids produced at 1600 rpm tool rotational speed and 45 mm/min tool travelling speed.

### 3.4. Tensile strength

During tensile test of the joints, the aluminum alloy was located on the fixed grip and PC was on the moving grip. The results of the tensile test of the joints with different tool speeds is shown in Fig. 6a.

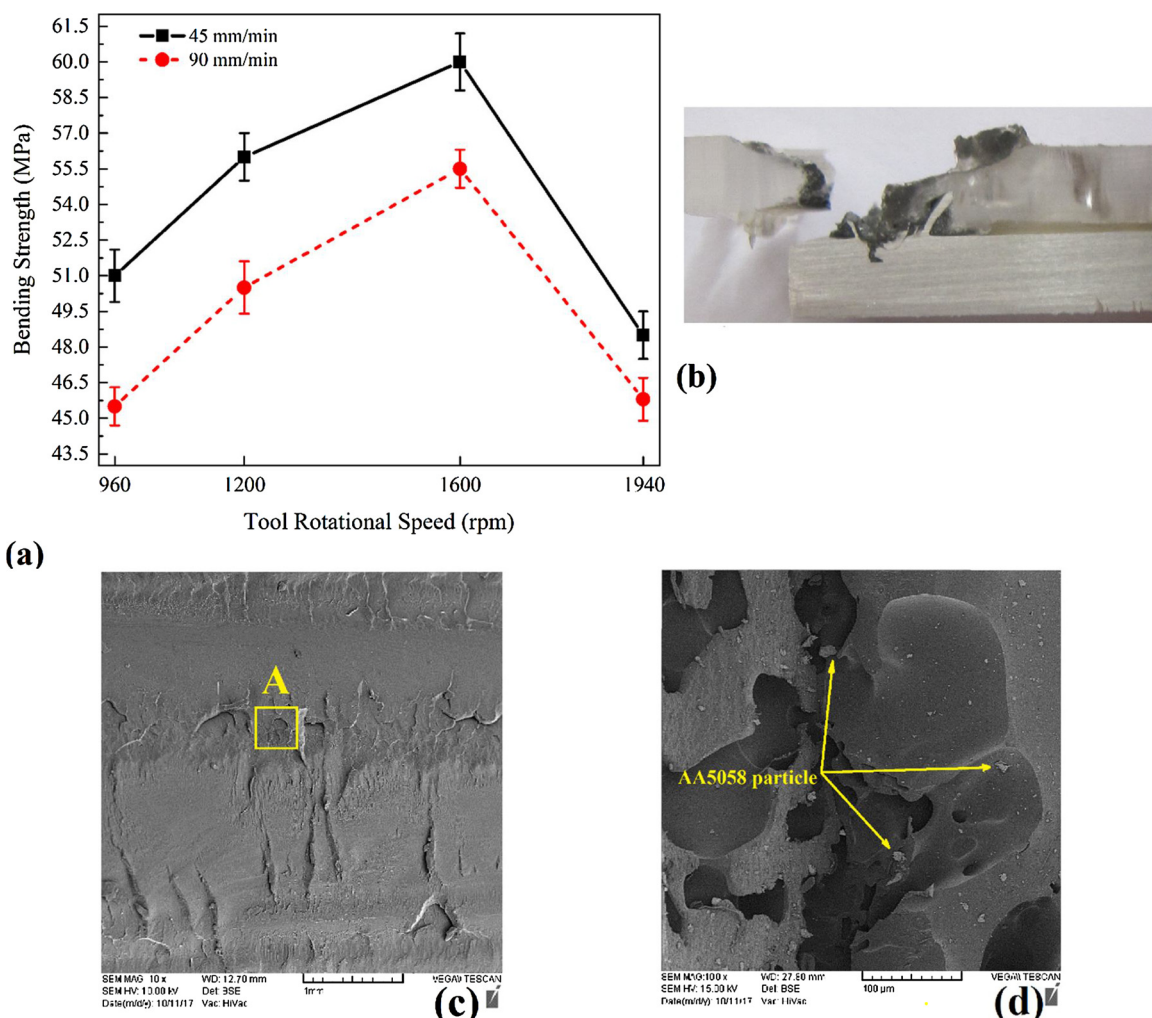


**Fig. 7.** (a) bending strength of joints, (b) electronic image from fractured bending sample, (c) low magnification SEM image from fracture surface, (d) high magnification SEM image from point (A) in fracture surface.

According to the results, by increasing the tool rotational speed, fracture force of joint increases till 1600 rpm and reduces after by. The ultimate tensile strength of joints welded at 960, 1200, 1600 and 1940 rpm and 45 mm/min tool speed were 40, 42, 46 and 39 MPa respectively. By dividing obtained tensile strength on raw PC (66.3 MPa), it can be found that the joint welded at 960, 1200 1600 and 1940 rpm and 45 mm/min tool speed had 60.3%, 63.3%, 69.4% and 54.2% of PC sheet tensile strength. The tensile strength of joints welded at 960, 1200, 1600 and 1940 rpm with 90 mm/min tool speed were 37, 39, 41 and 36 MPa respectively which stands for 55.8%, 58.8%, 61.8% and 54.2% of PC sheet's strength. The tensile sample reveals that tensile crack was initiated between the lower area of stir zone (interface of SZ and AA5058 alloy TMAZ) and final fracture occurred when the central crack fully separated the AA5058 alloy and PC sheets apart. This phenomenon reveals that the aluminum/polymer interface on the SZ was the weakest part of this joint. As discussed before changing of molecular weight, interaction bounding, formation of shrinkage bubble and gap directly affects the joint strength. The tensile test sample, broken sides of PC sheet and AA5058 aluminum alloy sides after tensile test are shown in Fig. 6b-d, respectively. The SEM image of fracture surface of PC side and aluminum side are shown in Fig. 6e and f, respectively. The high magnification SEM image from fracture surface of PC sheet shows tiny particle of AA5058 alloy stacked on polymer surface. In a recent work by Khodabakhshi et al. [34], the adhesion mechanism between the aluminum and polymer during FSW process proposed as the chemical interaction by the formation of aluminum oxide at the interface.

Some of adhered AA5058 alloy particles to the PC can be seen on the fracture surface. These fine particles are different from particles that were scattered in the PC bed by FSW tool.

During the tensile test, these particles separated from the aluminum TMAZ and the lower area of SZ (that is visible in SEM image). SEM macro-graph from the fracture surface of the tensile tested specimen in aluminum side revealed the skin peal AA5058 alloy surface which is produced with stirring action of FSW tool. The presence of PC clusters on the surface of the AA5058 alloy sheet indicated that the quality of chemical bonding between the polymer and AA5058 alloy in macro and micro scale is different. For more explanation, it can be mentioned that the bonding strength of PC/AA5058 alloy is higher than that of the strength of the re-solidified PC. By comparing the SEM images, it can be concluded that the polymer particles remained at the AA5058 aluminum fracture surface are larger than the aluminum particles sticking to the PC matrix.

### 3.5. Bending strength

The results of the bending tests of FSW samples is shown in Fig. 7a. The bending behavior showed that the fracture of all samples after test were located in SZ. An image of fracture location on a bending sample is shown in Fig. 7b. Due to the bending test results, joints which welded at 960, 1200, 1600 rpm and 1940 rpm with 45 mm/min tool speed had 51, 56, 60 and 48.5 MPa bending strength. By dividing obtained bending strength on raw PC's bending strength (88 MPa), it can be found that the

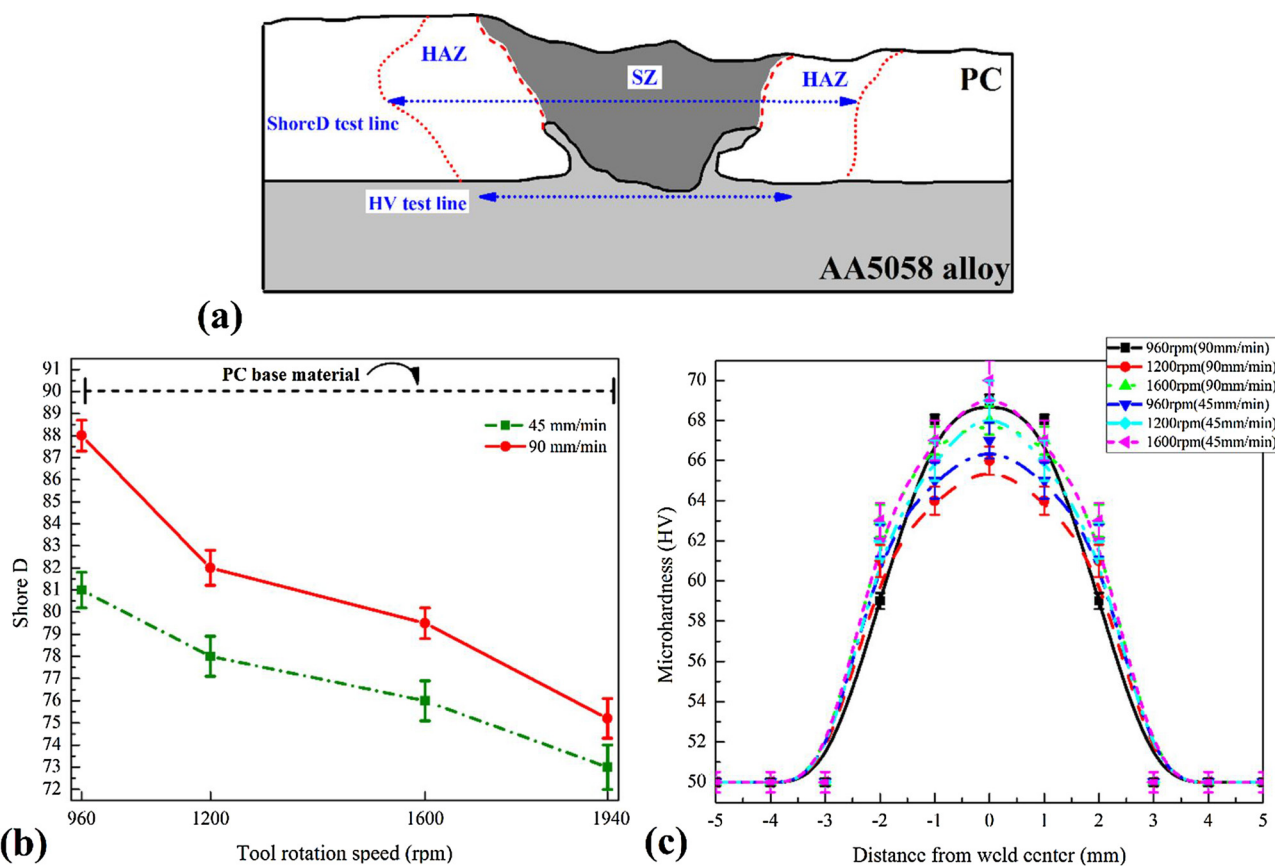


**Fig. 8.** (a) schematic view from hardness test line at PC and AA5058 alloy, (b) results of hardness changes (Shore D) in PC side, (c) results of hardness changes (HV) in AA5058 alloy side.

joints welded at 960, 1200, 1600 and 1940 rpm at 90 mm/min tool speed had 57.9%, 63.6%, 68.2% and 55.1% of PC sheet's bending strength. The bending strength of joints welded at 960, 1200, 1600 rpm and 1940 rpm with 90 mm/min tool speed were 45.5 MPa (51.7% bending strength of PC sheet), 50.5 MPa (57.3% bending strength of PC sheet), 55.5 MPa (63.0% bending strength of PC sheet), and 45.8 MPa (52.0% bending strength of PC sheet), respectively. The SEM image from fracture surface that had been shown in Fig. 7c, reveals that the smooth fracture path appears in upper area and then disordered crack propagation that is very similar to cleavage fracture, grows until the final rapture. The High magnification SEM image from boundary between smooth area and disordered crack propagation is shown in Fig. 7d. The results shows that shrinkage bubble caused the crack to change the growth mode. In addition aluminum particle does not have effective role in crack growth rate during the bending test.

### 3.6. Hardness test

The study of the hardness of the PC sheet after FSW can be informative with respect to the mechanical strength of the joints. Due to the selected hardness test for PC and existing aluminum particles in the SZ, it is not possible to make accurate measurements according to the Shore D but the general trend of hardness changes has been reported. During hardness test a straight line has been selected from HAZ area in advancing side to retreating side in the middle of the joint to determine the changes in the hardness of PC and AA5058 alloy.

Fig. 8a shows the schematic view of selected hardness test lines in PC and aluminum alloy. Fig. 8b and c presents the hardness variation of the FSW PC and AA5058 alloy at various tool rotational speeds, respectively. The results (Fig. 8b) shows that the hardness of PC after FSW decreases for all samples compared to primary raw PC sheet. According

to the results, by increasing the tool rotational speed, the hardness re-solidified PC in stir zone decreases in all samples. This may be related to molecular weight reduction of the PC, since the molten PC is affected by the frictional heat during the process [45–47]. The lowest hardness of FSW PC welded at 960, 1200, 1600 and 1940 rpm with 45 mm/min tool speed were 81, 79, 76 and 73 Shore D and for joints welded at 960, 1200, 1600 and 1940 pm with 90 mm/min tool speed were 88, 83, 80 and 76 Shore D, respectively. The hardness of AA5058 alloy also changed after FSW process. The fine graining of AA5058 alloy in HAZ and TMAZ are caused the micro-hardness of these places to increase. As can be seen in Fig. 8c, by increasing the heat input the micro-hardness of aluminum side grows. The results showed that the highest micro-hardness of aluminum side allocated to the joint welded at 1940 pm and 45 mm/min tool speed is ~77 HV and the lowest hardness produced on the joint welded at 960 rpm and 90 mm/min tool speed is ~63 HV, respectively.

### 4. Conclusions

The possibility of dissimilar friction stir welding between AA5058 aluminum alloy and polycarbonate (PC) in lap joint design was assessed. Different aspects and processing parameters were analysed to establish a suitable working window for fabrication of an Al-PC bimaterial structure. The main findings can be summarized as follow:

- In this joint, the weld zone formed as metal-polymer composite which contains spread AA5058 alloy particles into PC matrix. By increasing tool rotational speed, the amount of aluminum particles in stir zone will increase which leads to a darker colour of joint line. On the other hand, at low tool travelling speed, the size of the aluminum particles in stir zone became larger.

- Materials flow pattern mainly included the formation of a U-shape macro-lock from aluminum metal toward polymer side. These antennae increase the contact area between the AA5058 aluminum alloy and PC. Also, the formation of some indentation or teeth series at the interface surface beside the micro-sized mechanical interlocks assisted in the bonding between these dissimilar materials.
- Microstructural studies displayed the formation of HAZ and TMAZ region on AA5058 alloy side and HAZ on the PC side. Some micro-cracks observed at SZ in low heat input welding conditions. The biggest defect in SZ was shrinkage bubbles, although no indication of any voids or other defects in the SZ.
- The strongest dissimilar joint was processed at  $w = 1600$  rpm and  $v = 45$  mm/min. Welding in these conditions improved the tensile strength of dissimilar structure up to 46 MPa that had 69.4% of PC sheet's strength. In these parameters, the bending strength of joint reached close to 62.8% (60 MPa) of the raw PC's bending strength.
- The hardness of the PC after FSW decreased for all samples compared to the initial raw PC sheet, because of the molecular weight reduction of the PC due to the frictional heat during the process. The fine graining of AA5058 alloy in HAZ and TMAZ increased the micro-hardness of these places.

## References

- [1] Khodabakhshi F, Haghshenas M, Sahraeinejad S, Chen J, Shalchi B, Li J, et al. Microstructure-property characterization of a friction-stir welded joint between AA5059 aluminum alloy and high density polyethylene. *J Miner Mater Charact Eng* 2014;98:73–82.
- [2] Bozkurt Y. The optimization of friction stir welding process parameters to achieve maximum tensile strength in polyethylene sheets. *Mater Des* 2012;35:440–5.
- [3] Oliveira PHP, Amancio-Filho ST, dos Santos JF, Hage Jr. E. Preliminary study on the feasibility of friction spot welding in PMMA. *Mater Lett* 2010;64:2098–101.
- [4] Amancio-Filho ST, Bueno C, dos Santos JF, Huber N, Hage Jr. E. On the feasibility of friction spot joining in magnesium/fiber-reinforced polymer composite hybrid structures. *Mater Sci Eng: A* 2011;528:3841–8.
- [5] Bilici MK, Yükler Alı, Kurtulmuş M. 'The optimization of welding parameters for friction stir spot welding of high density polyethylene ssheets'. *Mater Des* 2011;32:4074–9.
- [6] Cole GS, Sherman AM. Lightweight materials for automotive applications. *J Miner Mater Charact Eng* 1995;35:3–9.
- [7] Amancio-Filho ST, dos Santos JF. Joining of polymers and polymer–metal hybrid structures: recent developments and trends. *Poly Eng Sci* 2009;49:1461–76.
- [8] David E, Lazar A. Adhesive bonding between aluminium and polytetra-fluoroethylene. *J Mater Process Technol* 2003;143–144:191–4.
- [9] Yusof F, Yukio M, Yoshiharu M, Abdul Shukor MH. Effect of anodizing on pulsed Nd:YAG laser joining of polyethylene terephthalate (PET) and aluminium alloy (A5052). *Mater Des* 2012;37:410–5.
- [10] Gruijic M, Sellappan V, Omar MA, Seyr N, Obieglo A, Erdmann M, et al. An overview of the polymer-to-metal direct-adhesion hybrid technologies for load-bearing automotive components. *J Mater Process Technol* 2008;197:363–73.
- [11] Aghajani Derazkola H, Aval HJ, Elyasi M. Analysis of process parameters effects on dissimilar friction stir welding of AA1100 and A441 AISI steel. *Sci Technol Weld Join* 2015;20:553–62.
- [12] Aghajani Derazkola H, Kashiry Fard R, Khodabakhshi F. Effects of processing parameters on the characteristics of dissimilar friction-stir-welded joints between AA5058 aluminum alloy and PMMA polymer. *Weld World* 2018;62(1):117–30.
- [13] Bergmann JP, Stambke M. Potential of laser-manufactured polymer-metal hybrid joints. *Phys Proc* 2012;39:84–91.
- [14] Berry DH, Namkanisorn A. Fracture toughness of a silane coupled polymer–metal interface: silane concentration effects. *J Adhes* 2005;81:347–70.
- [15] Matheny MP, Graff KF. 11 - ultrasonic welding of metals. In: Gallego-Juárez JA, Graff KF, editors. Power ultrasonics. Oxford: Woodhead Publishing; 2015. p. 259–93.
- [16] Yan P, Güngör ÖE, Thibaux P, Liebeherr M, Bhadeshia HKDH. Tackling the toughness of steel pipes produced by high frequency induction welding and heat-treatment. *Mater Sci Eng: A* 2011;528:8492–9.
- [17] Abibe AB, Amancio-Filho ST, dos Santos JF, Hage Jr. E. Mechanical and failure behaviour of hybrid polymer–metal staked joints. *Mater Des* 2013;46:338–3347.
- [18] Blaga L, Bancilă R, dos Santos JF, Amancio-Filho ST. Friction Riveting of glass-fibre-reinforced polyetherimide composite and titanium grade 2 hybrid joints. *Mater Des* 2013;50:825–9.
- [19] Lambiase F, Paoletti A. Friction-assisted clinching of Aluminum and CFRP sheets. *J Korean Soc Manuf Process Eng* 2018;31:812–22.
- [20] Balle F, Wagner G, Eifler D. Ultrasonic spot welding of aluminum sheet/carbon fiber reinforced polymer – joints. *Materwiss Werksttech* 2007;38:934–8.
- [21] Balle F, Wagner G, Eifler D. Ultrasonic metal welding of aluminium sheets to carbon fibre reinforced thermoplastic composites. *Adv Eng Mater* 2009;11:35–9.
- [22] Balle F, Eifler D. Statistical test planning for ultrasonic welding of dissimilar materials using the example of aluminum–carbon fiber reinforced polymers (CFRP) joints. *Materwiss Werksttech* 2012;43:286–92.
- [23] Goushegir SM, dos Santos JF, Amancio-Filho ST. Friction spot joining of aluminum AA2024/carbon-fiber reinforced poly(phenylene sulfide) composite single lap joints: microstructure and mechanical performance. *Mater Des* 2014;54:196–206.
- [24] Goushegir SM, dos Santos JF, Amancio-Filho ST. Influence of process parameters on mechanical performance and bonding area of AA2024/carbon-fiber-reinforced poly (phenylene sulfide) friction spot single lap joints. *Mater Des* 2015;83:431–42.
- [25] Mitschang P, Velthuis R, Didi M. Induction spot welding of Metal/CFRPC hybrid joints. *Adv Eng Mater* 2013;15:804–13.
- [26] He X, Gu F, Ball A. A review of numerical analysis of friction stir welding. *Prog Mater Sci* 2014;65:1–66.
- [27] Nandan R, DebRoy T, Bhadeshia HKDH. Recent advances in friction-stir welding – process, weldment structure and properties. *Prog Mater Sci* 2008;53:980–1023.
- [28] Mishra RS, Ma ZY. Friction stir welding and processing. *Mater Sci Eng R Rep* 2005;50:1–78.
- [29] Simar A, Bréchet Y, de Meester B, Denquin A, Gallais C, Pardoent T. Integrated modeling of friction stir welding of 6xxx series Al alloys: process, microstructure and properties. *Prog Mater Sci* 2012;57:95–183.
- [30] Yusof F, Miyashita Y, Seo N, Mutoh Y, Moshwan R. Utilising friction spot joining for dissimilar joint between aluminium alloy (A5052) and polyethylene terephthalate. *Sci Technol Weld Join* 2012;17:544–9.
- [31] Lambiase F, Paoletti A, Grossi V, Genna S. Improving energy efficiency in friction assisted joining of metals and polymers. *J Mater Proc Technol* 2017;250:379–89.
- [32] Lambiase F, Paoletti A, Genna S, Illio D. Friction assisted joining of aluminum and PVC sheets. *J Korean Soc Manuf Process Eng* 2017;29:221–31.
- [33] Lambiase F, Paoletti A. Mechanical behavior of AA5053/polyetheretherketone (PEEK) made by friction assisted joining. *Compos Struct* 2018;189(1):70–8.
- [34] Khodabakhshi F, Haghshenas M, Chen J, Shalchi Amirkhiz B, Li J, Gerlich A. Bonding mechanism and interface characterisation during dissimilar friction stir welding of an aluminium/polymer bi-material joint. *Sci Technol Weld Join* 2017;22:182–90.
- [35] Liu FC, Nakata K, Liao J, Hirota S, Fukui H. Reducing bubbles in friction lap welded joint of magnesium alloy and polyamide. *Sci Technol Weld Join* 2014;19:578–87.
- [36] Ratanathavorn W, Melander A. Dissimilar joining between aluminium alloy (AA 6111) and thermoplastics using friction stir welding. *Sci Technol Weld Join* 2015;20:222–8.
- [37] Shahmiri H, Movahedi M, Kokabi AH. Friction stir lap joining of aluminium alloy to polypropylene sheets. *Sci Technol Weld Join* 2016;22:120–6.
- [38] Huang Y, Meng X, Xie Y, Wan L, Lv Z, Cao J, et al. Friction stir welding/processing of polymers and polymer matrix composites. *Comp Part A: App Sci Manuf* 2018;105:235–57.
- [39] Elyasi M, Aghajani Derazkola H, Hosseiniadeh M. Investigations of tool tilt angle on properties friction stir welding of A441 AISI to AA1100 aluminium. *Proc IMechE, Part B: J Engineering Manufacture* 2016;230(7):1234–41.
- [40] Junior WS, Emmler T, Abetz C, Handge UA, Dos Santos JF, Amancio-Filho ST, et al. Friction spot welding of PMMA with PMMA/silica and PMMA/silica-g-PMMA nanocomposites functionalized via ATRP. *Polymer* 2014;55:5146–59.
- [41] Lambiase F, Paoletti A, Di Ilio A. Friction spot stir welding of polymers: control of plunging force. *Int J Adv Manuf Technol* 2017;90(9–12):2827–37.
- [42] Lambiase F, Paoletti A, Di Ilio A. Mechanical behaviour of friction stir spot welds of polycarbonate sheets. *Int J Adv Manuf Technol* 2016;87(5–8):2293–303.
- [43] Lambiase F, Paoletti A, Di Ilio A. Effect of tool geometry on loads developing in friction stir spot welds of polycarbonate sheets. *Int J Adv Manuf Technol* 2015;80(1–4):301–14.
- [44] Aghajani Derazkola H, Simchi A. Effects of alumina nanoparticles on the microstructure, strength and wear resistance of poly(methyl methacrylate)-based nanocomposites prepared by friction stir processing. *J Mech Behav Biol Mater* 2018;79:246–53.
- [45] Aghajani Derazkola H, Khodabakhshi F, Simchi A. Friction-stir lap-joining of aluminium-magnesium/poly-methyl-methacrylate hybrid structures: thermo-mechanical modelling and experimental feasibility study. *Sci Technol Weld Join* 2018;23(1):35–49.
- [46] Aghajani Derazkola H, Simchi A. Experimental and thermomechanical analysis of friction stir welding of poly(methyl methacrylate) sheets. *Sci Technol Weld Join* 2018;23(3):209–18.
- [47] Aghajani Derazkola H, Simchi A. Experimental and thermomechanical analysis of the effect of tool pin profile on the friction stir welding of poly(methyl methacrylate) sheets. *J Korean Soc Manuf Process Eng* 2018;34(A):412–23.